DOI https: //doi. org/10.1007/s11595-022-2492-2

Microstructure and Mechanical Properties of AlSiTiCrNiCu Particles Reinforced Al6061 Composites by SPS and HPS Process

WANG Zhijun[1], ZHOU Shengjie[3], SHAO Puzhen[1], SUN Kai[1], ZHANG Qiang[1,2*], XIU Ziyang[1,2*], XIAO Haiying[1,2*], WU Gaohui[1,2]

(1. School of Materials Science and Engineering, Harbin Institute of Technology, Harbin 150001, China; 2. Key Laboratory of Advanced Structure-Function Integrated Materials and Green Manufacturing Technology, School of Materials Science and Engineering, Harbin Institute of Technology, Harbin 150001, China; 3. Chengdu Holy Industry & Commerce Corp. Ltd. (Group), Chengdu 611936, China)

Abstract: Three groups of AlSiTiCrNiCu high entropy alloy (HEA) particles reinforced Al6061 composites were fabricated by spark plasma sintering at 520 and 570 ℃ (S520, S570) and by hot-pressed sintering at 570 ℃(H570). The AlSiTiCrNiCu (AST) particles used as reinforcements were synthesized by mechanical alloying. The influences of the sintering process on the microstructure and mechanical properties of composites were investigated. The results showed that the AST particles had a near-equiatomic composition with a single BCC structure. The sintering temperature and time had a coupling influence on the interfacial microstructure. S520 had hardly reaction products and slight interfacial diffusion, and the AST particles were completely high entropy. Intense interfacial reactions happened on S570 and H570 with the same reaction products. The element diffusion of S570 was focused on the edge of the AST particles with partial loss of high entropy. Complete element diffusion and entire loss of high entropy of AST particles happened on H570. The differences in the microstructure caused by the three preparation methods led to the changes in mechanical properties and fracture mechanisms of composites.

Key words: high entropy alloys; mechanical alloying; Al matrix composites; spark plasma sintering; hot-pressed sintering

1 Introduction

Aluminum matrix composites (AMCs) are composites with metals or alloys as matrix and particles, fibers, or whiskers as reinforcements. Reasonable process optimization enables the materials to have good ductility and processability of the matrix, as well as high specific strength and specific stiffness, good thermal conductivity, wear resistance, and dimensional stability of the reinforcements[1-5]. However, in the face of the rapid progress of manufacturing in the few years, the development of traditional ceramic reinforced aluminum composites has entered a bottleneck because the bonding strength of the interface between ceramic and matrix is hard to guarantee as well as the ceramic itself has serious defects leading to a decrease in the comprehensive mechanical properties of the composites[6-10]. In 2004, Yeh[11,12] broke the concept of traditional alloys in designing and preparing multi-components high entropy alloys (HEAs). HEAs are promising structural and functional materials due to their high strength, wear resistance, corrosion resistance, and special thermal and electromagnetic properties that are not available in conventional alloys, and their nature as metals makes it possible to have better interfacial compatibility with the aluminum matrix[13-15].

Recently, studies on using HEAs as reinforcements in composites have already been carried out. Karthik *et al*[16] first used frictional deposition for additive manufacturing of CoCrFeNi nanocrystalline HEA particles reinforced AA5083 composites. The fabricated 12 vol% HEA_p/AA5083 composite exhibited excellent microscopic properties. Fine nanocrystalline HEA distributed in the matrix uniformly, no brittle phase formed on the interface, and the forged aluminum

(Received: June 26, 2021; Accepted: Sept. 18, 2021)

WANG Zhijun(王智君): E-mail: hitzhijun@gmail.com

*Corresponding author: ZHANG Qiang(张强): Prof.; Ph D; E-mail: zhang_tsiang@hit.edu.cn; XIU Ziyang(修子扬): Assoc. Prof; Ph D; E-mail: xiuzy@hit.edu.cn; XIAO Haiying(肖海英): Assoc. Prof.; Ph D; E-mail: xyyhit@hit.edu.cn

Funded by the National Natural Science Foundation of China (Nos. 52071117, 51771063) and the Heilongjiang Provincial Science Fund for Distinguished Young Scholars (No. JQ2021E002)

matrix dynamically recrystallized to obtain an ultrafine crystal with well-dispersed second phase particles, which significantly improved the tensile strength and compressive strength of the composite. In another study, Liu *et al*[17] used SPS method for the fabrication of 5 vol% AlCoCrFeNi high-entropy alloy reinforced Al matrix composites. The research shows that a smooth interface between HEA reinforcement and the Al matrix could be generated at 540 ℃. Moreover, at a higher temperature of above 560 ℃, there was a melting of the particle-contacting zone between HEA and Al leading to the formation of the transition layer to a single FCC phase, of which the sickness increased with increasing sintering temperature. It could be found that the strengthening effect of the HEA particles in the Al matrix is mainly reflected by the element diffusion layer between HEA and matrix which can hinder the crack propagation[16-18]. Therefore, controlling the interface bonding state between the HEA particles and the Al matrix through process regulation can effectively improve the mechanical properties of the HEA/Al composites.

In this study, a novel AlSiTiCrNiCu high entropy system was chosen as a reinforcement and was prepared by mechanical alloying. Al6061 was selected as the matrix and a group of AlSiTiCrNiCu particles reinforced composites were firstly fabricated by SPS (spark plasma sintering) and HPS (hot-pressed sintering). The relationship between microstructures and mechanical properties of the composites were also investigated. Through the research of this article, new ideas will be provided for the preparation and strengthening mechanisms of AMCs.

2 Experimental

2.1 Synthesis of AlSiTiCrNiCu HEA particles

Commercial powders of Al, Si, Ti, Cr, Ni, Cu (400-mesh, 99.5 wt% purity, ZhongNuo Advanced Material (Beijing) Technology, China) with the composition of equiatomic were used as initial materials to synthesize AlSiTiCrNiCu HEA particles. The mixtures were sufficiently mixed for 24 h in a V-type mixer followed by a high-energy ball milling in a planetary ball mill (QM-3SP2, Nanjing University Instrument Factory, China) using stainless steel pot and balls to reach mechanical alloying. The pot was inflated with nitrogen then sealed before milling. A ball-to-powder weight ratio of 10:1 and a rotation speed of 350 rpm/min was applied. 15 min of milling was followed by 5 min of cooling to avoid excessive heat during mechanical alloying. A small number of powders was taken out at regular intervals of 10 h up to the total milling period of 40 h for microstructures and phase analysis, then the milled powders were taken out, vacuum dried for 2 h, separated by a 400-mech stand sieve, and vacuum sealed as reinforcement, as shown in Fig.1. In the following, the abbreviation AST particles was used to represent the AlSiTiCrNiCu particles.

2.2 Synthesis of AlSiTiCrNiCu-Al6061 composites

The samples used in this work were fabricated with Al6061 powders (10 μm, 99.5 wt% purity, Northeast Light Alloy, China) as matrix and AlSiTiCrNiCu powders prepared in advance as reinforcements in a volume ratio of 3: 97 and 5: 95. The powders were sufficiently mixed for 24 h in a V-type mixer as starting materials of composites. The composites were fabricated by SPS and HPS methods (Fig.1). For SPS, the composite powders were first cold pressed at 5 MPa for 5 min to obtain a preform, followed by spark plasma sintering under an argon atmosphere with a pressure of 40 MPa. The heating-up time was controlled at 12 min to reach the final sintering temperature, and the holding time was controlled at 10 min then being rapid cooled in the cooling room to obtain a composite bulk. The SPS temperatures were 520 ℃ and 570 ℃, respectively. For HPS, the composite powders were placed in steel mold (inner diameter is 100 mm) with both sides contacted with graphite plates (100 mm in diameter) and cold pressed at 5 MPa for 15 min followed by being heated in the furnace (570 ℃, argon atmosphere). Then the treated preform was pressed under 150 MPa for 30 min and air-cooled to obtain a composite bulk. Hereafter the abbreviated "Sxxx-v" or "Hxxx-v" was used to describe the composites (S and H respectively means the SPS and HPS method, xxx means the sintering temperature, v means the volume fraction of the reinforcement).

2.3 Tests and characterization

All sintered bulks were low temperature annealed at 340 ℃ for 1 h before mechanical properties tests and other characterizations. The density of composites was measured by Archimedes method using a precision analytical balance (BS 224B, Sartorius, Germany) while the Brinell Hardness was measured with a load of 250 kg and holding for 15 s (HB-3000, Fangyuan Testing Machine, China). The elastic modulus of composites was measured by impulse excitation of

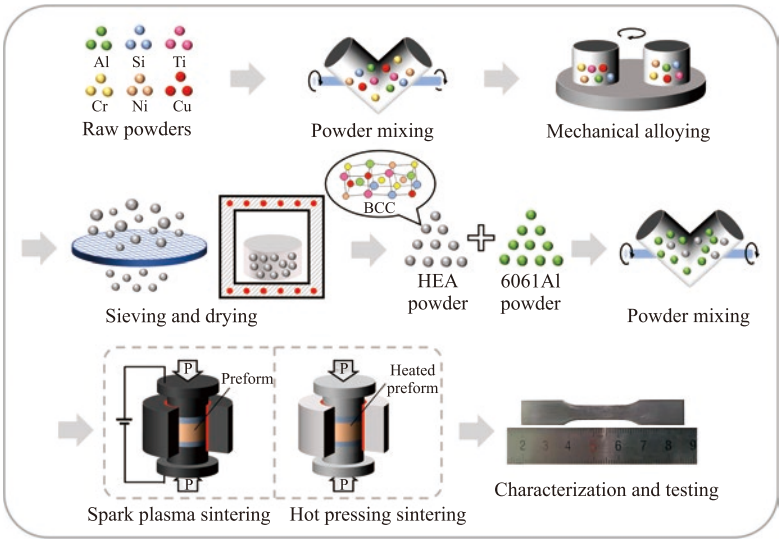

Fig.1 Schematic diagrams of preparation process of AlSiTiCrNiCu particles and its aluminum matrix composites (AMCs) as reinforcements

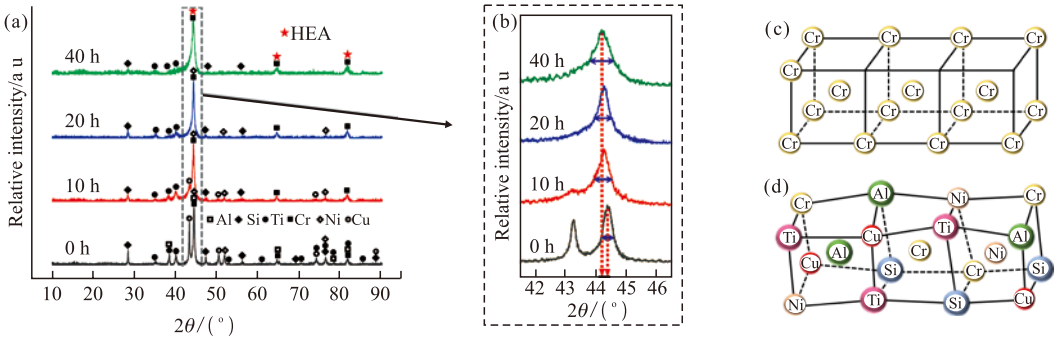

Fig.2 (a) XRD patterns of AiSiTiCrNiCu (AST) particles at different milling times; (b) enlarged image of the selected area in (a); Schematic diagrams of the BCC structure of (c) Cr element and (d) AST high entropy alloy

vibration (IET-01, ZhuoSheng Detection Instrument, China) using 3 mm × 4 mm × 36 mm samples. The room temperature tensile strength tests were conducted using a universal electronic mechanical tester (5569, Instron, USA), of which the displacement speed of the clamp is 0.5 mm/min, and the strain was measured using a capacitance extensometer. The surface of the tensile samples (Fig.1) was polished by sandpapers to eliminate wire-cutting marks before testing. A laser particle size analyzer (Masterizer 2000, Marven Panalytical, the UK) was used to measure the size of particles using deionized water as a dispersant. All the tests were repeated at least three times.

Phase analysis was carried out on a diffractometer (X'PERT, Panalytical, Dutch) with Cu Kα radiation and the spectra were collected in the range of 10°-90° (2θ) and a scanning speed of 6°/min. The morphology observation and elemental analyses were conducted on a field emission scanning electron microscope (SUPRA65, ZEISS, Germany) equipped with an energy dispersive spectrometer (EDS, Oxford, the UK). Additionally, metallographic samples were polished with sandpapers and chromium oxide turbid liquid. Further microstructure analysis was conducted on a transmission electron microscope. The sample was manually thinned to less than 40 μm and then etched by an ion beam milling machine (Gatan 695, the USA).

3 Results and discussion

3.1 Microstructure and phase constituent

3.1.1 AlSiTiCrNiCu particles

The XRD results of the AST powders with different milling times are shown in Fig.2(a). It can be found that the diffraction peaks of all composing elements were clearly distinguished at 0 h. However, after 10 h of milling, most of the initial peaks had weakened or disappeared and a significant broadening of the major peak (2$\theta \approx 44°$) took place and shifted to a lower angle, indicating the lattice expansion and the gradual formation of the solid solution phase[19,20], which could be observed in Fig.2(b) showing the

enlarged image of the selected area in Fig.2(a). In addition, the characteristic peaks of Cu ($2\theta \approx 43°$) and Ni ($2\theta \approx 52°$) had almost completely disappeared, while the intensity of Al peaks ($2\theta \approx 38°$) reduced observably, illustrating the Cu and Ni elements firstly dissolved into the lattice of the system followed by Al, which was due to the severe deformation enhanced diffusion[21,22]. The earlier dissolution of Al, Cu, and Ni elements can be explained by the higher diffusion coefficients of Al and Cu due to the lower melting points[20]. Furthermore, the lower value of the mixed enthalpy of Cu with other alloying elements is also the reason for its earlier alloying, and the ability to form an infinite solid solution with Cu allowing the Ni element to be alloyed earlier[23].

After milling for 20 h, the Al peaks($2\theta \approx 38°$) disappeared completely, while those of Ti ($2\theta \approx 40°$) and Si ($2\theta \approx 28°$) had slightly weakened, indicating the slow process of mechanical alloying for Si and Ti. Moreover, the major peak ($2\theta \approx 44°$) further broadened as shown in Fig.2(b) and the corresponding Cr-like BCC phase was found. According to the report that materials with higher melting points have higher bonding energies and lower diffusion coefficients, the Cr element in this article possesses the highest melting points which limited its serving as a solvent during mechanical alloying. And therefore, during the mechanical alloying process, the Cr atoms were replaced by other elements and the high entropy solid solution possessed a BBC structure similar to the Cr element[20,22]. Fig.2(c) and (d) are sketch maps showing the formation of solid solution with BCC structure based on Cr lattice.

When the milling time increased to 40 h, significant broadening of the major peaks could be observed as shown in Fig.2(b), which was attributed to the formation of nanocrystalline according to Scherrer's equation[24]. Moreover, the Si and Ti peaks were greatly reduced but had not completely disappeared, indicating the incomplete solution of Si and Ti elements into the high entropy system because of the unique cubic diamond structure of Si element and HCP structure of Ti element as well as the high melting points and large mixing enthalpies with other elements[19,20,23].

The surface morphologies of the particles milled for 0, 5, 10, 15, 20, and 40 h are shown in Fig.3(a-f). The original particles are characterized by various shapes such as spherical, rod-like, flaky, and other irregular shapes (Fig.3(a)). It is obvious that the particle size of the powders increased significantly at 5 h then decreased dramatically along with significant changes in the surface morphology with the prolonging of the milling time. It is known that, during the mechanical alloying process, violent deformation, work hardening, cold welding, and fracture would happen on the particles on account of the impact, extrusion, and shearing of the grinding ball[19,25].

At the very initial stage of milling (5 h), the shape of milled powders was irregular with remarkably large size to the range of 200 - 500 μm, which can be

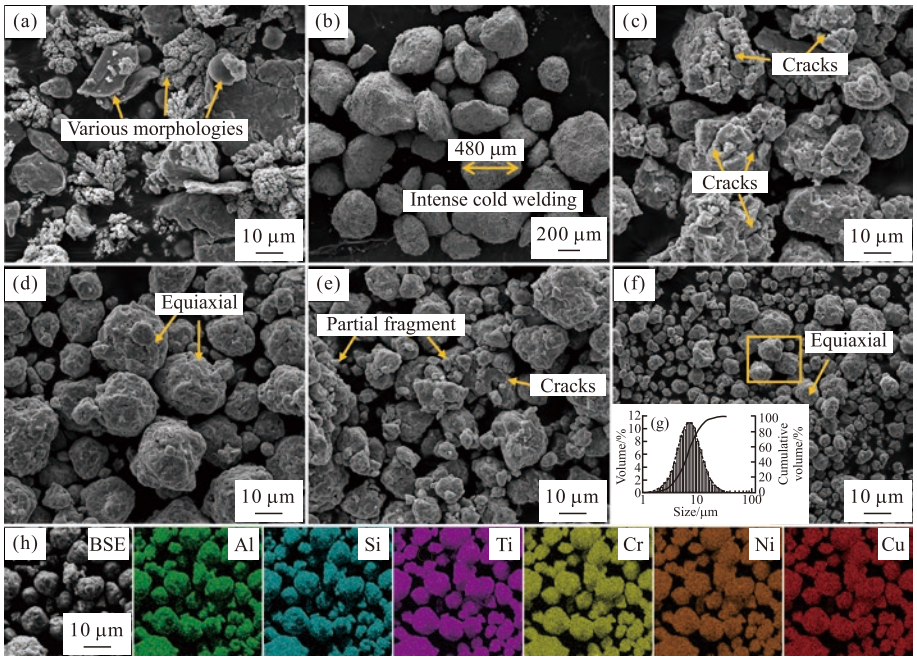

Fig.3 SEM images of particle morphologies at different milling time: (a) 0 h, (b) 5 h, (c) 10 h, (d) 15 h, (e) 20 h, (f) 40 h; (g) The particle size distribution of the as-milled particles; (h) EDS maps of the as-milled particles

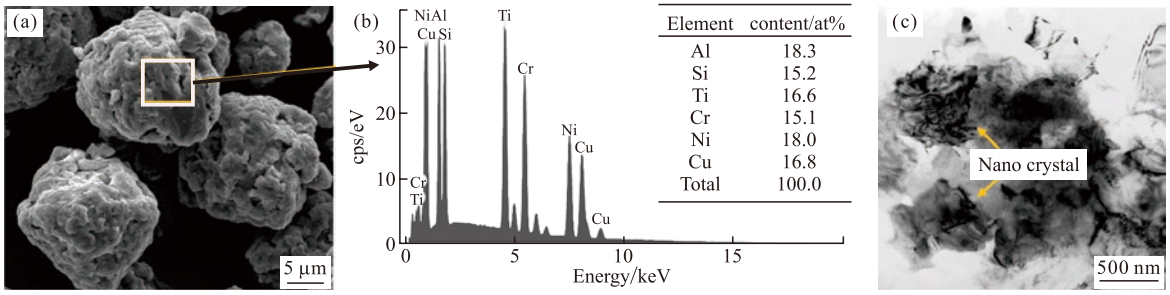

Fig.4 (a) SEM image of the as-milled particles (partially enlarged image of Fig.3(f)); (b) EDS analysis result of the selected area in (a); (c) TEM bright-field image of the particle

explained that the powders of different elements still maintained good deformation ability, which caused severe cold welding and led to an increase of particle size (Fig.3(b)). After 10 h of milling, the median size of particles was significantly reduced to 45.7 μm, and the surface of particles is quite rough, which should be caused by the adhesion of finer particles on the surface of larger ones. Obvious cracks on the particles should be caused by the weakening of deformation and work hardening of particles (Fig.3(c)). When the milling time increased to 15, 20, and 40 h, the continuous weakening of plastic deformation and cold-welding ability of particles induced cracks on the particles, and thus, a significant decrease of the particle size to the median diameter of 32.5, 15.4, and 7.2 μm, respectively (Fig.3(d-f)). Furthermore, the shape of particles became more closer to spherical, and the surface of particles became smoother. In addition, the refinement process of particles during mechanical alloying was always accompanied by atomic diffusion leading to phase transformation and formation of solid solution[20,25,26]. It can also be observed that the as-milled particles exhibit lognormal distribution according to Fig.3(g). The EDS mappings of the as-milled particles (40 h) (Fig.3(h)) showed that all constituent elements were evenly distributed in the particles.

The high magnification SEM image of the rectangle area in Fig.3(f) is shown in Fig.4(a) that the as-milled particles are nearly spherical with relatively coarse surfaces. Fig.4(b) is the EDS analysis result of the selected area in Fig.4(a) that the stoichiometric ratio of each constituent element is approximately equal to 1, indicating that the as-milled particles have the characteristic of high entropy[14,19]. Fig.4(c) presents the TEM bright-field image of a single AST particle, which is composed of many grains with a diameter of hundreds of nanometers. Therefore, the conclusion can be obtained that the as-milled AlSiTiCrNiCu particles with nanocrystalline were successfully synthesized by mechanical alloying.

3.1.2 AlSiTiCrNiCu- Al6061 composites

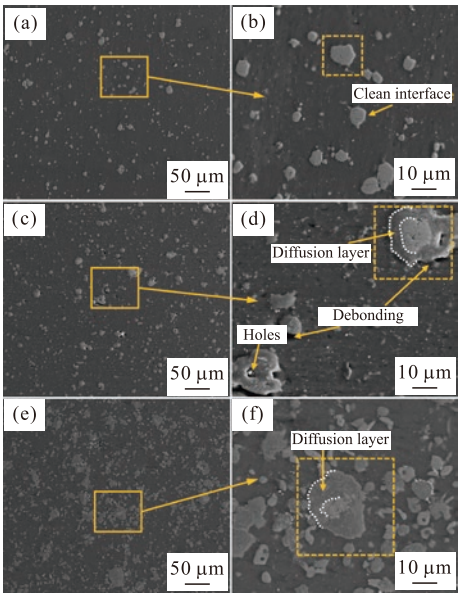

Fig.5 Representative second electron SEM microstructures of the polished surface of the AST particles/Al6061 composites: (a), (b) S520-5; (c), (d) S570-5 and (e), (f) H570-5

Three groups of $(AlSiTiCrNiCu)_p$/Al6061 composites (S520-3, S520-5; S570-3, S570-5; H570-3, H570-5) were fabricated by SPS at 520 and 570 ℃ and by HPS at 570 ℃. SEM images of S520-5, S570-5, and H570-5 are shown in Fig.5(a-f), showing good dispersion of AST particles in the Al6061 matrix. At higher magnifications (Fig.5(a), (c), (e)), it is evident that S520-5 had almost no interfacial bonding layer because the interface between AST particles and matrix was quite clean (Fig.5(b)). As for S570-5, it could be observed from Fig.5(c) and (d) that the morphology of AST particles changed greatly compared to S520-5 with a relatively thick diffusion layer caused by severe element diffusion between AST particles and matrix. Furthermore, large numbers of holes are formed at the boundaries between the AST particles and the matrix as well as on the AST particles themselves (Fig.5(d)),

and the holes generated at the boundaries could also induce local debonding between AST particles and matrix. However, for H570-5, the morphology of AST reinforcements was quite different from the other two methods above and completely different from the original as-milled AST particles, but no holes were observed at the interface or on the reinforcements and the edges of particles were smoother than S570-5 (Fig.5(e) and (f)), as the elements in AST particles diffused more intensely and more drastically than S570-5 due to longer sintering time of HPS method. Diffusion layers between white dotted lines in Fig.5(d) and (f) showed that the diffusion behavior in H570-5 was more serious than in S570-5.

The difference in the interface morphology among S520-5, S570-5, and H570-5 could be explained by combining the sintering temperature, sintering time, and local high temperature. As S520-5 had a lower sintering temperature and the same sintering time compared with S570-5, conclusions could be obtained that the ability for element diffusion of SPS methods is mainly controlled by temperature. The holes generated in S570-5 (Fig.5(d)) could be explained that the SPS method will cause the local melting between particles to be more intense with the increase of temperature than traditional powder metallurgy, not only resulting in a gradient on thermal expansion of the particles but also leading to an intense increase in the difference in thermal expansion coefficient between the AST particles and the matrix inducing a significant increase in interfacial stress. In addition, the sintering time of SPS was too short to guarantee that the holes mentioned above were filled due to the fluidity and plastic deformation of the powder during sintering[27,28]. And thus, because of the much longer sintering time of the HPS method, adequate element diffusion and powder lowing could be determined, and therefore, much fewer holes were generated. The same reason could also explain the smooth edges of AST particles in H570-5.

The XRD patterns of S520-5, S570-5, and H570-5 are shown in Fig.6. For S520-5, most of the reinforcement particles in the matrix still retained the characteristics of high entropy, and the phase compositions were mainly composed of Al and HEA by XRD analysis, indicating that no serious interfacial reaction occurred because of the lower sintering temperature. For S570-5 and H570-5, the diffraction peaks corresponding to the AST particles can hardly be detected and many peaks of new phases appeared by XRD analysis, proving that the AST particles underwent severe reaction at 570 ℃, and thus, many new phases were generated, which means that the AST particles can react with Al at elevated temperature and the interfacial reactions are mainly controlled by sintering temperature. Moreover, despite the difference in the metallographic morphologies between S570-5 and H570-5, the peaks of the two composites are quite the same despite the local high temperature due to SPS.

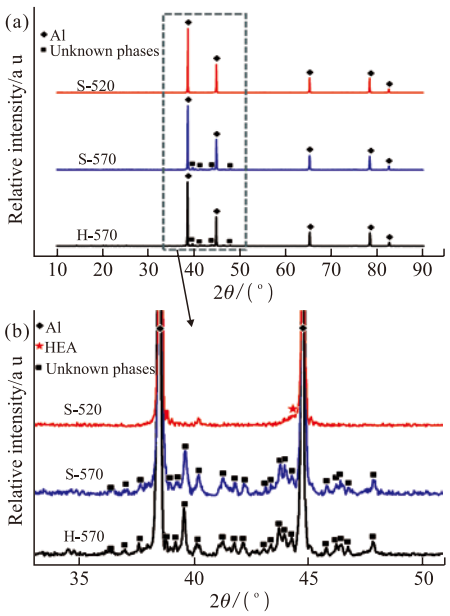

Fig.6 (a) XRD patterns of S520-5, S570-5, and H570-5 and (b) magnified zone marked in (a)

3.2 Interface diffusion layer

The EDS mappings of the areas surrounded by the dotted lines in Fig.5(b), (d), (f) are shown in Fig.7(a-c), showing the representative elemental interdiffusion behavior at the interface of S520, S570, and H570, respectively. The EDS results of the rectangular areas in Fig.7(a-c) (Ⅰ, Ⅱ, Ⅲ, Ⅳ, Ⅴ, and Ⅵ) are respectively plotted in Fig.9(a-f). For S520, there was a significant elemental boundary between the AST particles and the matrix (Fig.7(a)), and no obvious element diffusion layer could be observed. Fig.9(a) and (b) illustrated that element in Ⅱ remained near-equiatomic, confirming the high entropy character, while the majority of Al in area Ⅰ further clarified the elemental boundary mentioned above.

For S570, it could be found that the interdiffusion behavior of elements between AST particles and matrix was extremely serious with a significantly thicker diffusion layer than S520 and the interdiffusion mainly occurred on the very edge of the particles. Moreover, the diffusion behaviors of elements were various, and different elements were segregated in different regions

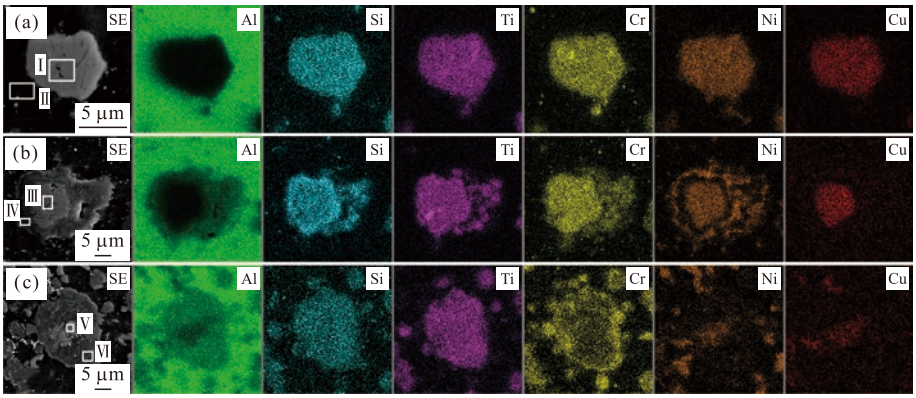

Fig.7 EDS mappings of (a) S520-5, (b) S570-5, and (c) H570-5

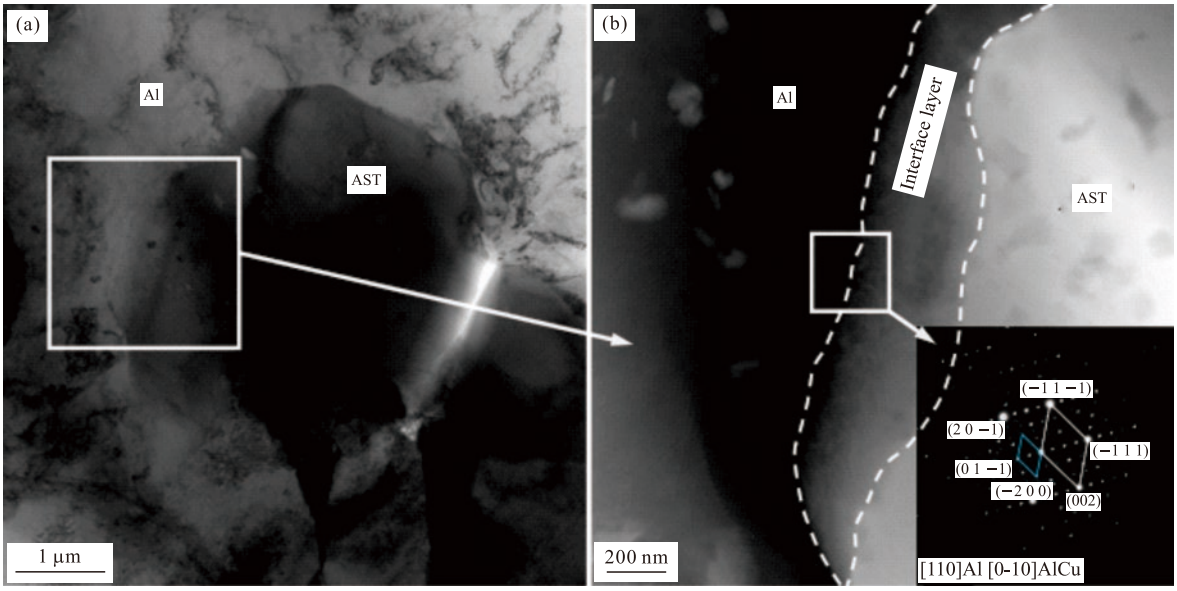

Fig.8 TEM images of S570: (a) bright-filed image of the interface; (b) HADDF image of the rectangle region marked in (a)

(Fig.7(b)). In this condition, Al was mainly exited in the matrix with a thick diffusion layer between the matrix and AST particle; Si occupied the initial AST particle zone with higher content in the diffusion layer on the edge; Ti and Cr stayed in the initial AST one with no apparent diffusion layers on the edge; Ni performed an exotic diffusion behavior as segregation regions were separated by poor layer, and thus, the segregation regions of Si and Ti on the edge of particles were complementary; Cu diffused violently into the matrix and just occupied the very center of the initial AST particle zone. Fig.9(c) confirmed that the interior of particles still retained high entropy, while Fig.9(d) illustrated the loss of high entropy in the edge of particles. The strong edge effect of element diffusion in S570 may be due to the local high temperature of the sintered neck by SPS, and the short diffusion time of elements because of the inadequate sintering time. The TEM images of S570 are presented in Fig.8. Fig.8(b) shows the HADDF image acquired from the enlarged interface region in Fig.8(a). It can be observed that a clear interface diffusion layer between Al and AST exists. The indexed SEAD pattern shows that there is AlCu phase between Al and the interface. However, the reaction in this study is complex with many kinds of interface products, and therefore, further work is needed to analyze all the products.

For H570, element diffusion behavior is more intense and complete than the other two methods without significant edge effects (Fig.7(c)). A large amount of Al in the matrix diffused into the AST particles, showing an obvious concentration gradient; Si and Ti mainly occupied the initial AST particle zone with no edge segregation of Si as in Fig.7(b); however, Cr performed differently with a small degree of segregation on the edge; the diffusion of Ni and Cu was quite intense with only a small part of the element-rich region in the center of particles. Fig.9(e) also confirmed the high entropy character in the very center of particles, yet Fig.9(f) verified the intense diffusion

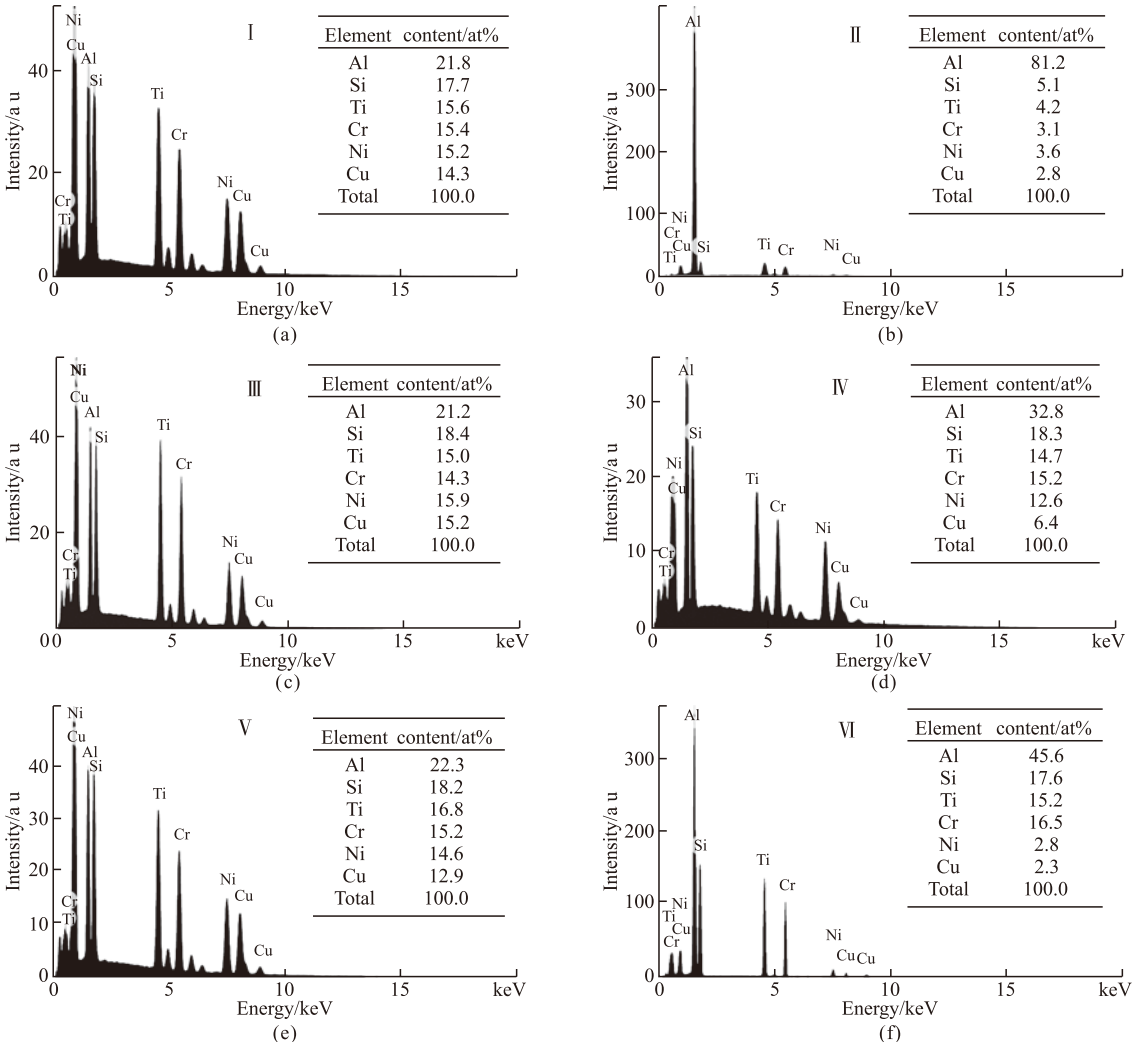

Fig.9 EDS analyses of zone Ⅰ, Ⅱ, Ⅲ, Ⅳ, Ⅴ, and Ⅵ in Fig.7, respectively

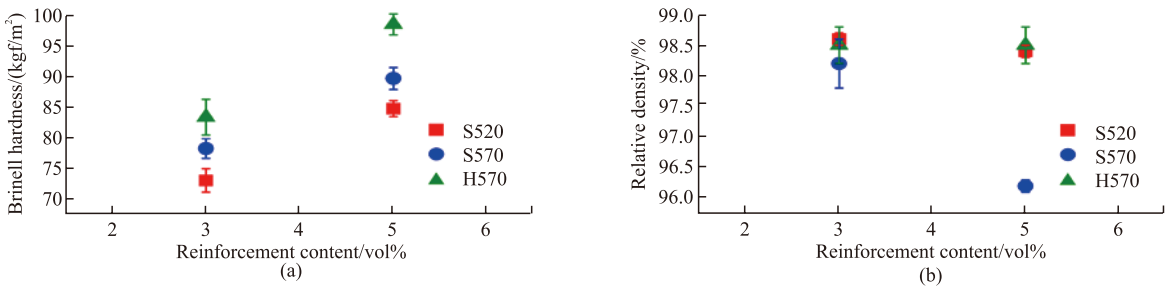

Fig.10 (a) Brinell hardness and (b) relative density of AST particles/Al6061 composites

of Al, Ni, and Cu. The sufficient sintering time of HPS gave a longer diffusion time for elements, which led to the intense diffusion of some elements.

3.3 Mechanical properties

The relative density and Brinell hardness of AST particles/Al6061 composites of different sintering methods and reinforcement contents are plotted in Fig.10. The hardness of composites enlarges greatly with increasing reinforcements contents, but the regularity of relative density is opposite as shown in Fig.10(a). All composites are possessed with high relative densities more than 96%. The relative density follows the rules of H570 > S520 > S570, and the relative density of S570-5 is smaller than other composites according to Fig.10(b). The relative densities of composites are strictly consistent with the metallographic images in Fig.5 that the holes generated at S570 have the main responsibility for the reduction of relative density. In addition, higher contents of AST particles introduced more interfaces,

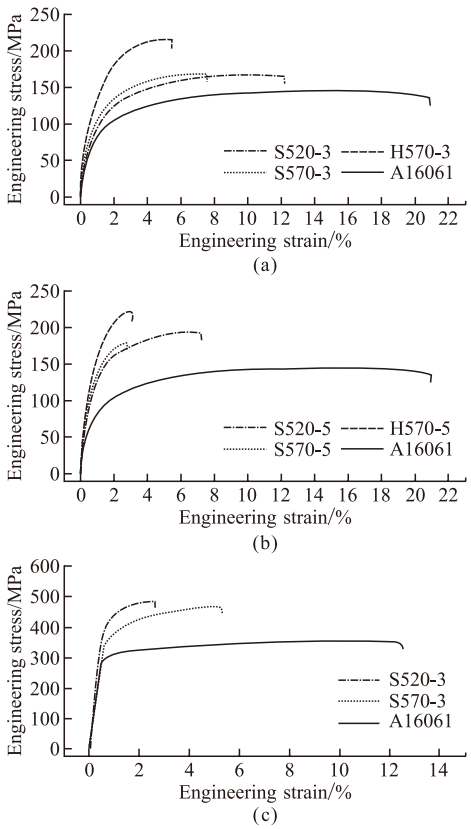

Fig.11 Room temperature tensile stress-strain curves of composites: (a) S520-3, S570-3 and H570-3 (as-annealed); (b) S520-5, S570-5 and H570-5 (as-annealed); (c) S520-3 and S520-5 (T6)

and resulted in more interfacial holes, as shown in Fig.5(d). The comparatively higher relative densities of H570 are because of the longer sintering time and more adequate densification degree of the HPS method. The Brinell hardness follows the rules of H570 > S570 > S520. The hardness of AMCs is related to both the densification degree of composites and the content of reaction products[1,29,30]. According to the XRD analysis (Fig.6), a large number of reaction products can be generated at S570 and H570, which may increase the hardness of composites. For H570, both a high degree of densification and intense interfacial reaction have positive effects on the hardness of the composites, so that the hardness values of HPS-3 and HPS-5 are the highest. For S570, the densification degree has fewer effects than the interfacial reaction, leading to the medium hardness of composites. Moreover, the reason that Brinell hardness increased with increasing AST particles contents for all the three groups of composites can be explained using Orowan dislocation strengthening theory: the reinforcements particles could restrain the deformation of the Al6061 matrix because of the dislocation bypassing mechanism[1,31,32], and thus, harder interfacial reaction products and better interfacial bonding could improve the hardness of composites.

The elastic moduli of the AST particles/Al6061 composites are plotted in Fig.12(a). It can be seen that the elastic modulus follows the rules of H570 > S570 > S520 and increase with increasing AST content. It was reported that the elastic modulus of AMCs is related to the efficiency of load transferred from the matrix to the reinforcements, and higher load transformation often leads to a high elastic modulus[32]. When the interface is clean without reaction products as shown in Fig.7(a), the elastic modulus is low. Conversely, when the interface is full of reaction products and exists as a band-like region as shown in Fig.7(b) and (c), the

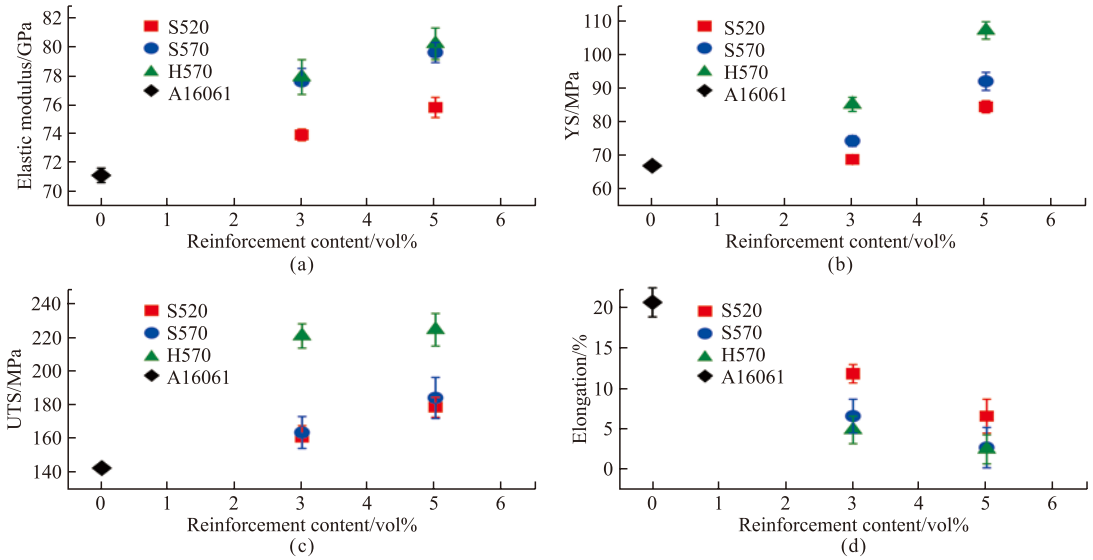

Fig.12 Room temperature mechanical properties of composites (as-annealed): (a) elastic modulus, (b) yield strength, (c) ultimate tensile strength, and (d) elongation

elastic modulus is high[32]. However, the development of holes in the interface will also lead to a decrease in elastic modulus, which can also explain that the elastic modulus of S570 is slightly smaller than H570[33].

The typical tensile stress-strain curves at room temperature of as-annealed 3 vol% and 5 vol% composites are illustrated in Fig.11(a) and (b), respectively, and the relevant mechanical properties are plotted in Fig.12. It is illustrated that, with the increase of AST content, the ductility corresponding to three sintering methods all decreased (Fig.12(d)), while the ultimate tensile strength (UTS) increased (Fig.12(c)). This is because the AST alloy in this article is a kind of brittle high entropy alloy[34,35], and hence, the increase of AST particles contents could manifestly reduce the ductility of the matrix. In addition, the increase in UTSs of S570 and H570 is not evident, which is attributed to the interfacial brittle phases and defects. For 3 vol% composites, it can be seen from Fig.11(a) that elongation follows the regularity of Al6061 > S520-3 > S570-3 > H570-3 (Fig.12(d)). Compared with Al6061, the plasticity of S570-3 and H570-3 reduced drastically, while S520-3 still retained relatively good ductility of 11.7%.

In addition, the UTS follows the opposite regularity of H570-3 > S570-3 > S520-3 > Al6061, and the H570-3 exhibited great improvement of UTS (220.1 MPa) compared with the matrix (142.2 MPa), but the improving effects of S520-3 and S570-3 are not obvious (Fig.12(c)). Similar regularities can also be seen in Fig.11(b) except for the intense plasticity reduction of S570-5. It is worth noting that the comprehensive mechanical properties of S570-3 and S570-5 are poor with low elongation and low UTS, which can be explained by the cracks in the AST particles themselves and the boundaries between AST particles and matrix as shown in Fig.5(d). The high UTS growth rates of H570 are related to the violent element interdiffusion behavior and the generation of new brittle phases, which were also attributed to the lower ductility compared with S520.

The strengthening effect of AST particles in the matrix is evaluated by yield strength (YS), as plotted in Fig.12(b). It is shown that the elastic modulus follows the rules of H570 > S570 > S520 and increases with increasing AST content. As mentioned above, the interface of S520 is clean with almost no reaction products that cannot play the role of transforming load, and thus, the load shared on the AST particles is not enough, which causes lower YS of S520[36]. As for the H570 and S570, the reaction layer (Fig.7(b) and (c)) could effectively bridge the AST particles and the matrix, leading to a more effective load transformation[29,37]. And therefore, the AST particles could effectively share the load, leading to higher YS. Similarly, holes on the interface of S570 can also

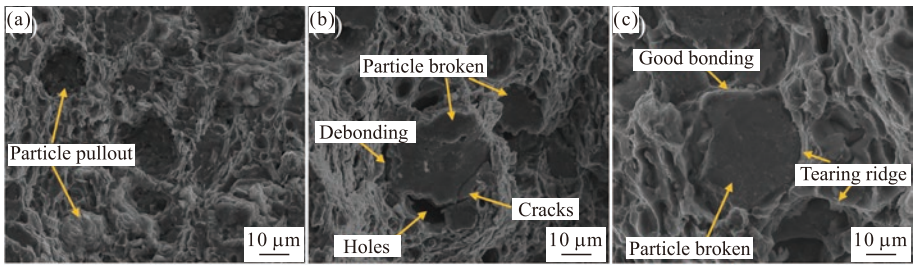

Fig.13 Room temperature tensile morphologies of (a) S520-3, (b) S570-3, and (c) H570-3

Table 1 Mechanical properties of as-annealed and T6 Al6061 and composites

Materials	Elastic modulus/GPa	Elongation/%	Yield strength/MPa	Ultimate tensile strength/MPa
Al6061 as-annealed	71.1	20.5	66.8	142.2
S520-3 as-annealed	73.9	11.7	68.7	160.5
S520-5 as-annealed	75.8	6.5	84.4	178.1
S570-3 as-annealed	77.6	6.5	74.2	163.2
S570-5 as-annealed	79.6	2.6	91.8	183.6
H520-3 as-annealed	77.9	4.8	85.1	220.1
H520-5 as-annealed	80.2	2.4	107.0	223.8
Al6061 T6	—	11.0	306.6	356.1
S520-3 T6	—	6.3	362.4	473.8
S520-5 T6	—	2.4	413.5	507.7

explain the lower YS of S570 than H570[33].

The results above indicate that S520 composites have better comprehensive mechanical properties, and the AST particles still remained intact with high entropy characteristics. Thus, T6 treatment of S520 was conducted, and the room temperature tensile stress-strain curves (Fig.11(c)) showed that the T6 treated S520-3 and S520-5 had a yield strength of 362.4 and 413.5 MPa, an ultimate tensile strength 472.4 and 509.3 MPa, and an elongation of 6.3% and 2.4%, indicating a large increase in UTS and YS. The mechanical properties of Al6061 and composites in the state of as annealed and T6 are listed in Table 1.

3.4 Fracture mechanism

Fig.13 shows the room temperature tensile fracture surface morphologies of S520-3, S570-3, and H570-3. It can be observed that the fracture morphologies of the composites mainly consist of the reinforcement particles being peeled off from the matrix or broken by themselves, dimples, or tearing ridges of the Al6061 matrix. For S520-3, nearly equiaxed pits and protrusions can be observed as shown in Fig.13(a), which is because of the particles being pulled out from the matrix. In addition, large numbers of dimples existed on the matrix, indicating the ductile fracture mode of S520-3. While, for S570-3, it is illustrated in Fig.13(b) that no obvious particles peeled-off can be observed, instead, the AST particles themselves fractured with flattened fracture surface. Furthermore, the AST particles were surrounded by a large number of holes, and thus, the holes gradually merged during the tensile process, causing the partial debonding between reinforcements and matrix. Few cracks can also be observed on the inside of AST particles. Fracture of reinforcement particles and flattened fracture surface of particles can also be observed in H570-3, as shown in Fig.13(c), except that no holes or debonding existed around the particles. In addition, there is a large number of tearing ridges in the matrix instead of the dimples in Fig.13(a).

The differences in fracture morphologies of three composites mainly depend on the strength of the interface between AST particles and matrix, which in general is positively correlated with the degree of interfacial reaction and element diffusion. During the loading process of composites, the stress acting on the matrix can be transferred to the reinforcements through the interface, thereby improving the yield strength (YS) and the ultimate tensile strength (UTS). The stress transformed through the interface increases with the increasing external load. For S520, the interface was weakly bonded with lower strength than AST particles. When the stress on the interface gradually increased to be larger than the interfacial bonding strength, it could cause the debonding of the interface and the peeled off of AST particles. But at this time, the value of stress on the interface is still low and in some areas is even lower than the yield strength of the matrix, resulting in the matrix still with the characteristics of ductile fracture and lower YS of composites. For S570, the interface was well bonded with higher strength than AST particles, but with few holes existed. When the load was transferred through the interface, the stress concentrated near the holes, eventually leading to the original cracks in the AST particles and the matrix. As the load increased, those cracks further expand until instability, causing the fracture of AST particles and the matrix. In this case, due to the stress concentration of the holes, the failure occurred when the stress on the interface was still at a low level, resulting in the relatively low YS and elongation, which leads to low UTS. For H570, the interface was clean and well bonded with higher strength than the AST particles. At this time, the load transferred to the reinforcements through the interface reaching a level much higher than the YS of the matrix and caused the fracture of AST particles. Therefore, the matrix fractured rapidly after the AST particles was broken, resulting in a large number of tearing ridges.

4 Conclusions

The AlSiTiCrNiCu HEA particles obtained by mechanical alloying was used as the reinforcements, and Al6061 was used as the matrix. The $(AlSiTiCrNiCu)_p$/Al6061 composites with reinforcement fractions of 3 vol% and 5 vol% were fabricated by SPS and HPS at 520 ℃. The effects of the sintering process on the microstructure and mechanical properties of composites were investigated. The conclusions are as follows:

a) AlSiTiCrNiCu HEA nanocrystalline particles with near-equiatomic composition were obtained by mechanical alloying, which is mainly composed of single-phase Cr-like BCC solid solution structure.

b) Sintering temperature and time were the main factors that affect the interface reaction and diffusion behavior of the composites. S520 had almost no reaction, while S570 and H570 had the same reaction products. No obvious element diffusion happened on

S520, and the AST particles were completely high entropy. Significant edge-focused element diffusion happened on S570 with partial loss of high entropy of the AST particles. Sufficient element diffusion happened on H570, and the high entropy of the AST particles was completely lost.

c) S520 had the best plasticity due to the absence of interface reaction. H570 had the highest elastic modulus, YS, and UTS because of the intense element diffusion and high interfacial bonding strength. The comprehensive mechanical properties of S570 were weak because of the holes at the interface.

References

[1] Ibrahim I A, Mohamed F A, Lavernia E J. Particle Reinforced Metal Matrix Composites–A Review[J]. *J. Mater. Sci*., 1991, 26: 1 137-1 156

[2] Miracle D B. Metal Matrix Composites-from Science to Technological Significance[J]. *Compos. Sci. Technol*., 2005, 65: 2 526-2 540

[3] Rawal S. Metal-Matrix Composites for Space Applications[J]. *JOM*, 2001, 53: 14-17

[4] Rosso M. Ceramic and Metal Matrix Composites: Routes and Properties[J]. *J. Mater. Process. Technol*., 2006, 175: 364-375

[5] Kaczmar J W, Pietrzak K, Włosiński W. The Production and Application of Metal Matrix Composite Materials[J]. *Mater. Process. Technol.*, 2000, 106: 58-67

[6] Dursun T, Soutis C. Recent Developments in Advanced Aircraft Aluminium Alloys[J]. *Mater. Des*., 2014, 56: 862-871

[7] Bdodunrin M O, Alaneme K K. Aluminium Matrix Hybrid Composites: A Review of Reinforcement Philosophies; Mechanical, Corrosion and Tribological Characteristics[J]. *J. Mater. Res. Technol.*, 2015, 4: 434-445

[8] Koli D K, Agnihotri G, Purohit R. Advanced Aluminium Matrix Composites: The Critical Need of Automotive and Aerospace Engineering Fields[J]. *Mater. Today Proc*., 2015, 2(4): 3 032-3 041

[9] Yashopal, Sumankant, Jawalkar C S, *et al.* Fabrication of Aluminium Metal Matrix Composites with Particle Reinforcement: A Review[J]. *Mater. Today Proc*., 2017, 4: 2 927-2 936

[10] Topcu I, Gulsoy H O, Kadioglu N, *et al.* Processing and Mechanical Properties of B_4C Reinforced Al Matrix Composites[J]. *J. Alloys Compd.*, 2009, 482: 516-521

[11] Yeh J W, Chen S K, Lin S J, *et al.* Nanostructured High-Entropy Alloys with Multiple Principal Elements: Novel Alloy Design Concepts and Outcomes[J]. *Adv. Eng. Mater.*, 2004, 6: 299-303

[12] Yeh J W, Chen S K, Gan J Y, *et al*. Formation of Simple Crystal Structures in Cu-Co-Ni-Cr-Al-Fe-Ti-V Alloys with Multiprincipal Metallic Elements[J]. *Metall. Mater. Trans*., 2004, A35: 2 533-2 536

[13] Yeh J W. Recent Progress in High Entropy Alloys[J]. *Ann. Chim. Sci. Mater.*, 2006, 6: 633-648

[14] Yeh J W. Alloy Design Strategies and Future Trends in High-Entropy Alloys[J]. *JOM*, 2013, 65: 1 759-1 771

[15] Zhang Y, Yang X, Liaw P K. Alloy Design and Properties Optimization of High-Entropy Alloys[J]. *JOM*, 2012, 64: 830-838

[16] Karthika G M, Panikarb S, Janaki Rama G D, *et al.* Additive Manufacturing of an Aluminum Matrix Composite Reinforced with Nanocrystalline High-Entropy Alloy Particles[J]. *Mater. Sci. Eng. A Struct.*, 2017, 679: 193-203

[17] Liu Y Z, Chen J, Li Z, *et al.* Formation of Transition Layer and Its Effect on Mechanical Properties of AlCoCrFeNi High-Entropy Alloy/Al Composites[J]. *J. Alloys. Compd.*, 2019, 780: 558-564

[18] Wang Z W, Yuan Y B, Zheng R X, *et al.* Microstructures and Mechanical Properties of Extruded 2024 Aluminum Alloy Reinforced by FeNiCrCoAl$_3$ Particles[J]. *Trans. Nonferrous Met. Soc. China*, 2014, 24: 2 366-2 373

[19] Vaidya M, Muralikrishna G M, Murty B S. High-Entropy Alloys by Mechanical Alloying: A Review[J]. *J. Mater. Res*., 2009, 34: 664-686

[20] Tian L H, Fu M, Xiong W. Microstructural Evolution of AlCoCrFeNiSi High-Entropy Alloy Powder during Mechanical Alloying and Its Coating Performance[J]. *Materials*, 2018, 11: 320

[21] Zhang K B, Fu Z Y, Zhang J Y, *et al.* Nanocrystalline CoCrFeNiCuAl High-Entropy Solid Solution Synthesized by Mechanical Alloying[J]. *J. Alloys. Compd*., 2009, 485: L31-L34

[22] Chen Y L, Hu Y H, Tsai C W, *et al.* Structural Evolution During Mechanical Milling and Subsequent Annealing of Cu–Ni–Al–Co–Cr–Fe–Ti Alloys[J]. *Mater. Chem. Phys*., 2009, 118: 354-361

[23] Takeuchi A, Inoue A. Classification of Bulk Metallic Glasses by Atomic Size Difference, Heat of Mixing and Period of Constituent Elements and Its Application to Characterization of the Main Alloying Element[J]. *Mater. Trans.*, 2005, 46: 2 817-2 829

[24] Varalakshimi S, Kamaraj M, Murty B S. Synthesis and Characterization of Nanocrystalline AlFeTiCrZnCu High Entropy Solid Solution by Mechanical Alloying[J]. *J. Alloys. Compd*., 2008, 460: 253-257

[25] Suryanarayana C. Mechanical Alloying and Milling[J]. *Prog. Mater. Sci.*, 2001, 46: 1-184

[26] Laurent-Brocq M, Goujon P A, Monnier J, *et al.* Microstructure and Mechanical Properties of a CoCrFeMnNi High Entropy Alloy Processed by Milling and Spark Plasma Sintering[J]. *J. Alloys. Compd*., 2019, 780: 856-865

[27] Mamedov V. Spark Plasma Sintering as Advanced PM Sintering Method[J]. *Powder Metall.*, 2002, 45: 322-328

[28] Guillon O, Gonzalez-Julian J, Dargatz B, *et al.* Field-Assisted Sintering Technology/Spark Plasma Sintering: Mechanisms, Materials, and Technology Developments[J]. *Adv. Eng. Mater.*, 2014, 16: 830-848

[29] Ramesh C S, Keshavamurthy R, Channabasappa B H, *et al.* Microstructure and Mechanical Properties of Ni–P Coated Si_3N_4 Reinforced Al6061 Composites[J]. *Mater. Sci. Eng. A Struct.*, 2009, 502: 99-106

[30] Wang S, Zhu S, Cheng J, *et al.* Microstructural, Mechanical and Tribological Properties of Al Matrix Composites Reinforced with Cu Coated Ti_3AlC_2[J]. *J. Alloys. Compd*., 2017, 690: 612-620

[31] Bagheri G A. The Effect of Reinforcement Percentages on Properties of Copper Matrix Composites Reinforced with TiC Particles[J]. *J. Alloys. Compd*., 2016, 676: 120-126

[32] Fei W D, Jiang X D, Li C, *et al.* Effect of Interfacial Reaction on the Young's Modulus of Aluminium Borate Whisker Reinforced Aluminium Composite[J]. *J. Mater. Letter.*, 1996, 15: 1 966-1 968

[33] Nardone V C. Assessment of Models Used to Predict the Strengthening of Discontinuous Silicon Carbide Reinforced Aluminum Alloys[J]. *Scr. Metall.*, 1987, 21: 1 313-1 318

[34] Yurchenko N Yu, Stepanov N D, Shaysultanov D G, *et al.* Effect of Al Content on Structure and Mechanical Properties of the $Al_xCrNbTiVZr$ (x = 0; 0.25; 0.5; 1) High-Entropy Alloys[J]. *Mater. Charact.*, 2016, 121: 125-134

[35] Li W D, Liaw P K, Gao Y F. Fracture Resistance of High Entropy Alloys: A Review[J]. *Intermetallics*, 2018, 99: 69-83

[36] Luan B F, Wu G H, Liu W, *et al.* High Strength Al_2O_{3p}/2024Al Composites-Effect of Particles, Subgrains and Precipitates[J]. *Mater. Sci. Technol.*, 2005, 21: 1 440-1 443

[37] Gao F, Xu C, P Zhang H, *et al.* Core-Shell Structured Al-Matrix Composite with Enhanced Mechanical Properties[J]. *Mater. Sci. Eng. A Struct.*, 2016, 657: 64-70